https://doi.org/10.1016/j.scriptamat.2016.01.035

Melt Spinning Synthesis of *p*-type Skutterudites: Drastically Speed Up the Process of High Performance Thermoelectrics

Lijie Guo[a], Guiwen Wang[a], Kunling Peng[a,b], Yanci Yan[a], Xiaodan Tang[a], Min Zeng[c,d], Jiyan Dai[c], Guoyu Wang[b], Xiaoyuan Zhou*[a]*

[a]College of Physics, Chongqing University, Chongqing 401331, People's Republic of China.

[b]Chongqing Institute of Green and Intelligent Technology, Chinese Academy of Sciences, Chongqing 400714, People's Republic of China.

[c]Department of Applied Physics, The Hong Kong Polytechnic University Kowloon, Hong Kong.

[d]Institute for Advanced Materials and Guangdong Provincial Key Laboratory of Quantum Engineering and Quantum Materials，South China Normal University, Guangzhou 510006, China.

Abstract:

In this study, via a home-made induction melting process combined with spark plasma sintering technique, we successfully synthesize the nanostructured skutterudites $Nd_xYb_yFe_3CoSb_{12}$ (x+y=1.0, x=0.3, 0.4, 0.5, 0.6, 0.7) in less than 3 h, which is significantly faster than that of the solid state reaction (168 h) and the traditional melt spinning method (40 h). Systematical microstructures analysis of the sintered bulk materials reveals the largely refined matrix grains (100-300 nm) and ubiquitous YbSb precipitates (~30 nm), resulting in a very low lattice thermal conductivity. A peak *ZT* up to 1.02 at 760 K is obtained for $Nd_{0.6}Yb_{0.4}Fe_3CoSb_{12}$ compound.

Keywords: *P*-type filled skutterudites; Melt-spinning; Phonon scattering; Thermoelectric properties

Rapidly growing of energy consumption is causing serious environmental problems. To solve these problems, thermoelectric (TE) devices having been considered as a new means to reduce the fuel consumption because of their ability to directly convert waste heat into useful electric power in a clean manner [1-8]. The conversion efficiency of thermoelectric device is determined by the dimensionless figure of merit ZT of the thermoelectric material which is defined as $ZT = (S^2\sigma/\kappa)T$, where σ, S, T, and κ ($\kappa = \kappa_e + \kappa_l$) are the electrical conductivity, Seebeck coefficient, absolute temperature and thermal conductivity, respectively. Ideal TE materials should have high electrical transport performance ($S^2\sigma$) and very low thermal conductivity (κ) at an appropriate temperature. Among them, filled skuterudites have attracted great deal of attention as one of the most potential thermoelectric materials. This is due to the fact that the filled skuterudites belong to the so-called phonon glass electron crystal (PGEC) [9-14], which is a concept being introduced during the last decade.

To date, the maximum ZT achieved is ~1.7 in *n*-type $CoSb_3$ based triple-filled skutterudites $Ba_{0.08}La_{0.05}Yb_{0.04}Co_4Sb_{12}$ [15]. However, the ZT values for *p*-type filled skutterudites mostly remain below unity. It is well-known that thermoelectric power generation devices require excellent and comparable performance for both *n*-type and *p*-type materials. Therefore, to enhance the thermoelectric performance of *p*-type skutterudites compounds has been an urgent task in the research field of thermoelectrics. Recently, L. N. Zhou *et al*. synthesized Yb/La double-filled *p*-type skutterudites and reported a peak ZT of 0.99 at 700 K in $Yb_{0.25}La_{0.6}Fe_{2.7}Co_{1.3}Sb_{12}$ [16]. G. J. Tan *et al*. synthesized Ce-filled *p*-type skutterudites and reported a peak ZT of

1.0 at 800 K in $Ce_{0.9}Fe_{3.4}Co_{0.6}Sb_{12}$[17]. R. H. Liu *et al*. synthesized Ce/Yb double-filled *p*-type skutterudites and reported a peak *ZT* of 1.02 at 700 K in $Ce_{0.6}Yb_{0.4}Fe_3CoSb_{12}$ [18].

Although the values of *ZT* for *p*-type skutterudites having been steadily increased, it is still much lower compared to *n*-type skutterudites. Meanwhile, to the best of our knowledge, the above-mentioned materials were mainly synthesized by the solid state reaction method (designated as SS). The time and energy were consumed largely in this process, where at least 168 h was needed for a typically take to merely prepare a compacted bulk. Thus, a quick and efficient process in a manner adaptable to industrial production is desired to synthesize thermoelectric materials with the favorable microstructure to hinder phonons transport without seriously degrading the electrical transport properties. One such effective technique is to fabricate nanostructured skutterudites compounds by melt spinning combined with spark plasma sintering (MS-SPS) due to the factors: (a) the melt spinning technology does reduce the processing period at a significant extent; (b) this rapid synthesis frequently yields uniformly dispersed nanoscaled precipitates, resulting in an additional mechanism to enhance the Seebeck coefficient and further lowering the thermal conductivity through filtering lower energy carriers and enhancing the phonons scattering[19,20]. Recently, Tang *et al*. reported an excellent performance in *p*-type skutterudites. A peak *ZT* of 0.89 at 800 K was obtained in $CeFe_4Sb_{12}$, which was synthesized in a relatively short time by the traditional melt spinning followed by spark plasma sintering (TMS-SPS) [21]. However, in this method, an ingot previously

made by solid states reaction is required for the following melt spinning processing. As driven by the market, further reduction of the fabrication time and cost is imperative.

In this paper, we employed a home-made melt spinning system assembled inside the glove box to rapidly fabricate $Nd_xYb_yFe_3CoSb_{12}$ (x+y=1.0, x=0.3, 0.4, 0.5, 0.6, 0.7) compounds. Instead of starting from a previously made ingot, in this method, we directly start the melt spinning processing from the raw materials. Compared to the SS and TMS-SPS processes, the current processing time is significantly reduced from 168 h and 40h to less than 3 h. More importantly, a significantly improved thermoelectric performance can be achieved from this method. The enhanced thermoelectric performance of the *p*-type Fe_3CoSb_{12}-based skutterudites $Nd_xYb_yFe_3CoSb_{12}$ compounds together with the dramatically reduced processing time are promising to the commercial-scale production for TE power generation application.

Samples with nominal compositions $Nd_xYb_yFe_3CoSb_{12}$ (x+y=1.0, x=0.3, 0.4, 0.5, 0.6, 0.7) were prepared via a home-made induction melting assembled inside the glove box combined with spark plasma sintering technique. Stoichiometric quantities of the constituent high purity elements Fe (pieces 99.99%), Co (slugs and foil 99.99%), Sb (chunk 99.9999%), Nd (ingot 99.99%) and Yb (ingot 99.99%) were weighed according to the each nominal composition.

All constituents were placed into a quartz tube and heated up to 1223 K till being melted via a home-made induction melting system, and meanwhile samples were

rotated via vortex caused by electromagnetic force. The obtained homogeneous samples were soaked at 1223 K for 15 min, and then blew out under 0.7 MPa and cooled by a rapid rotating copper roller with a speed of 25 rad/s to get supercooled ribbon-shaped material. All the above operations were done inside a glove box to prevent any contamination of oxygen. The as-prepared ribbons were subsequently grounded into powder and loaded into a graphite die of 10 mm diameter in size and then sintered by spark plasma sintering (SPS-625) at 833 K under a pressure of 45 MPa for 5 min. The finished samples possess a density greater than the theoretical value of 95% and the whole process is less than 3 h.

Powder X-ray diffraction (XRD) study on the samples was carried out using PANalytical X'pert apparatus with Cu K_α radiation. The morphology and microstructure of the sample were investigated using field emission scanning electron microscopy (SEM, JSM-7800F, JEOL) and transmission electron microscopy (TEM, JEOL 2100F). The Seebeck coefficient (S) and electrical conductivity (σ) were measured at temperature from 300 to 840 K on rectangular-shape samples by a commercial apparatus (LSR-3) under the protective atmosphere of argon. Thermal conductivity (κ) was calculated according to the equation $\kappa=\lambda C_p d$, where λ is the thermal diffusivity measured by the laser flash method (LFA, 457, Netzsch) at temperatures from 300 to 823 K, C_p is the specific heat obtained by differential scanning calorimetry (DSC, 404 F3, Netzsch). Sample density d was calculated with archimide method. During all the measurements, the samples were under the atmosphere of argon to prevent oxidation at elevated temperatures.

Figure 1(a) displays the powder XRD patterns of the sintered $Nd_xYb_yFe_3CoSb_{12}$ (x+y=1.0, x=0.3, 0.4, 0.5, 0.6, 0.7) samples prepared by melt spinning combined with spark plasma sintering (MS-SPS) and the solid state reaction method (SS). It is noted that almost all the diffraction peaks can be indexed to the skutterudites phase, indicating that a single phase of filled skutterudites has been successfully obtained in all samples. However, a trace amount of impurity phase $FeSb_2$ can be detected in the XRD patterns mainly due to the phase decomposition induced by charge imbalance for $Nd_{0.4}Yb_{0.6}Fe_3CoSb_{12}$ and $Nd_{0.7}Yb_{0.3}Fe_3CoSb_{12}$ compounds [22]. Figure 1(b) shows the lattice parameters of $Nd_xYb_yFe_3CoSb_{12}$ compounds prepared by MS-SPS and SS, where the inset is an expanded view of the XRD pattern for specific angles between 69.5° to 70.5°. We noted a gradual shift of 2θ to lower angles with increasing Yb concentration, indicating an increase of lattice parameters due to the increased content of fillers as reported in the literature [22].

Figures 2(a) and (b) show the typical SEM images of the freshly fractured surface of sintered SS and MS-SPS samples, respectively. It is apparent that these samples are closely packed possessing clean and sharp grain boundaries. These structural characteristics should be beneficial to charge transport properties. It is worth noting that the grain size of our MS-SPS sample (100~300 nm) is more uniform and smaller in contrast to that of the SS sample (3~10 um). As a consequence, for the MS-SPS sample, the significantly refined grain size is believed to be able to strongly scatter long-wavelength phonons, providing an extra potential mechanism to reduce the lattice thermal conductivity[23].

Detailed microstructures of the $Nd_{0.3}Yb_{0.7}Fe_3CoSb_{12}$ samples prepared by MS-SPS was studied by means of transmission electron microscopy (TEM), and the low-magnification image is shown in Figure 2 (c), where more nanoscale precipitates can be observed. Figure 2(d) shows a representative high-resolution transmission electron microscopy (HRTEM) image of one spherical/ellipsoidal precipitate in a grain outlined by dotted lines. The electron beam for the HRTEM image is along the [001] zone axis, and from the HRTEM image shown in Figure 2(e), the interplanar distance of this nanoscale precipitate is can be determined to be 3.07 Å, which is indeed very close to the $d_{(200)}$ lattice spacing (theoretical value is 3.04 Å) for YbSb compound. Scanning transmission electron microscopy (STEM) in combination with energy dispersive X-ray (EDX) spectroscopy can be used to probe the element concentration of the precipitates in contrast to the matrix of $Nd_{0.3}Yb_{0.7}Fe_3CoSb_{12}$. Although it is difficult to quantitatively determine the exact composition of individual precipitates because of their overlapping with the matrix, EDX analysis as shown in Figures 2 (f) and (g) can still qualitatively indicate a large increase in the Yb/Sb contents and a significant decrease in Fe/Co contents from the precipitates compared to the matrix regions. Considering the above two factors revealed by TEM, it is believed that these spherical/ellipsoidal precipitates embedded in skutterudite grains prepared by MS-SPS are mainly YbSb nanoscaled precipitates. This result is completely different from that reported in literature [21], where an impurity phase of $FeSb_2$ was observed in *p*-type skutterudites $CeFe_4Sb_{12}$ synthesized by tradition melt-spinning method. It is worth noting that these precipitates are coherently

orientated with the matrix, acting as effective scattering centers to enhance the scattering for mid-to-long wavelength phonons, providing an extra mechanism to further reduce the lattice thermal conductivity [23, 24-26].

Figure 3 shows temperature-dependent electrical conductivity (σ), Seebeck coefficient (S), and power factor ($PF=S^2\sigma$) of the $Nd_xYb_yFe_3CoSb_{12}$ (x+y=1.0, x=0.3, 0.4, 0.5, 0.6, 0.7) compounds measured at temperatures from 300 to 840 K. For easy comparison, the data of SS sample for $Nd_{0.3}Yb_{0.7}Fe_3CoSb_{12}$ are also presented. As shown in Figure 3 (a), the electrical conductivity decreases with increasing of temperature, indicating that all specimens are degenerate semiconductors as reported in literature[27]. In addition, the electrical conductivity decreases with increasing of Nd content, this can be attributed to the decrease of carrier concentration except for the $Nd_{0.7}Yb_{0.3}Fe_3CoSb_{12}$ sample. As shown in Table I, one can find that the reason why the $Nd_{0.7}Yb_{0.3}Fe_3CoSb_{12}$ sample has a lower electrical conductivity than other samples is because of its lower carrier mobility instead of lower carrier concentration. It is believed that the presence of second phase $FeSb_2$ as observed in XRD pattern for the $Nd_{0.7}Yb_{0.3}Fe_3CoSb_{12}$ sample may result in the reduction of carrier mobility. In addition, it is noted that: (a) the electrical conductivity of the $Nd_xYb_yFe_3CoSb_{12}$ compounds prepared by MS-SPS is lower than that of the SS sample, (b) the electrical conductivity of the $Nd_{0.3}Yb_{0.7}Fe_3CoSb_{12}$ sample (the representative of MS-SPS samples) is also lower than the TMS-SPS sample as shown in the inset of Figure 3 (a). Such a reduction is attributed to the fine microstructures of MS-SPS samples, where the increased grain boundary density enhances carrier scattering, leading to the lower

carrier mobility.

In Figure 3 (b), the positive Seebeck coefficient indicates that the majority of charge carriers are holes. The Seebeck coefficient increases with increasing of temperature and reaches peak values at temperatures from 760 to 790 K. Afterwards, the Seebeck coefficient decreases due to the presence of an intrinsic semiconducting behavior. In addition, as expected, the Seebeck coefficient increases with the increased content of Nd due to the decreased carrier concentration. Moreover, the Seebeck coefficient of MS-SPS samples for $Nd_xYb_yFe_3CoSb_{12}$ is higher than that of the SS sample and the TMS-SPS sample.

The power factor of all samples at temperatures ranging from room temperature to 785 K is plotted in Figure 3(c). One can see that the $Nd_{0.6}Yb_{0.4}Fe_3CoSb_{12}$ sample has the highest power factor compared to the remaining samples. However, above 785 K, the $Nd_{0.5}Yb_{0.5}Fe_3CoSb_{12}$ sample possesses the highest power factor reaching a maximum value of 2.7 mW $K^{-2}m^{-1}$ at 810 K owing to its higher electrical conductivity. On the other hand, compared to the SS sample, the power factor for the MS-SPS $Nd_{0.3}Yb_{0.7}Fe_3CoSb_{12}$ compound is higher by 28% at room temperature and by 56% at 840 K due to the larger Seebeck coefficient. However, the power factor of MS-SPS $Nd_{0.3}Yb_{0.7}Fe_3CoSb_{12}$ sample is lower than TMS-SPS sample.

The thermal transport properties of the sintered bulk MS-SPS and SS samples were measured and presented in Figure 4. As shown in Figure 4(a), the thermal conductivities of all MS-SPS samples first decrease with increase of temperature and then increase; such trends are mainly manipulated by lattice thermal conductivity at

first and then the electrical thermal conductivity. Moreover, the total thermal conductivity decreases with increasing Nd amount till x is up to 0.6. Further increasing Nd fillers to 0.7, the thermal conductivity presents reverse behavior. This is attributed to the reduction of the electronic thermal conductivity is more significant than the increase of the lattice thermal conductivity. As such, proper amount of Nd / Yb fillers are effective in reducing the thermal conductivity of *p*-type skutterudites compounds. In contrast, the thermal conductivities of MS-SPS samples are much lower than the SS and TMS-SPS samples. This can be attributed to the reduction of the lattice thermal conductivity due to the enhanced phonons scattering.

The lattice thermal conductivity κ_l is subsequently calculated by subtracting the electronic part κ_e from the total thermal conductivity κ. As shown in Figure 4(b), one can see that the lattice thermal conductivity κ_l decreases with the increase of temperature and then increases when the temperature is above 720 K. This is attributed to the appearance of the bipolar diffusion effect. In addition, the κ_l decreases with the increase of Yb amount, and the specific explanation is as follows: Ab-initio calculation has been performed to explore the resonant frequencies of various fillers in *p*-type skutterudites[18]. It shows that w_0 of Nd and Yb along the < 111 > direction in *p*-type Fe_3CoSb_{12}-based skutterudites are 62 cm^{-1} and 51 cm^{-1}, respectively. Generally speaking, the low-frequency lattice phonons contribute most to the heat conduction in solids. As such, it is expected that Yb is more efficient than Nd in reducing the lattice thermal conductivity in filled skutterudites. This which is in good agreement with our experimental observation, where the continuously lowered κ_l is

observed with the increasing of Yb in our $Nd_xYb_yFe_3CoSb_{12}$ compounds. In addition, it is noted that κ_l of MS-SPS samples are remarkably lower than that of SS sample. As an example, the lattice thermal conductivity for the $Nd_{0.3}Yb_{0.7}Fe_3CoSb_{12}$ sample is reduced by 23% at room temperature and by 25% at 823 K. This reduction is reasonably attributed to: (a) a rational combination of fillers can be considered to reduce the κ_l by introducing additional resonant phonon scattering; (b) the melt spinning processing leads to a formation of grains with much finer microstructures and a larger quantity of boundaries strongly scattering long-wavelength phonons; (c) numerous YbSb nanoscaled precipitates in the MS-SPS samples act as effective scattering centers that block the propagation of mid-wavelength phonons; (d) dislocations and point defects introduced by the nonequilibrium melt spinning process that scatter shorter-wavelength phonons[29]. All the above mentioned scattering mechanisms result in this vast reduction of the lattice thermal conductivity in our $Nd_xYb_yFe_3CoSb_{12}$ compounds.

The temperature dependence of dimensionless figure of merit *ZT* is plotted in Figure 4 (c). The *ZT* values of MS-SPS samples are enhanced in the whole temperature range as compared to the SS sample, primarily due to its improved power factor and largely reduced thermal conductivity. The maximum *ZT* value reaches 1.02 for the MS-SPS $Nd_{0.6}Yb_{0.4}Fe_3CoSb_{12}$ compound at 760 K. Meanwhile, it is noted that *ZT* value of the $Nd_{0.3}Yb_{0.7}Fe_3CoSb_{12}$ MS-SPS sample is higher by 75% and 7% at 760 K than that of the SS and TMS-SPS samples, respectively. However, the average *ZT* value（ZT_{ave}）is considered as more accurate to compare the performance of

thermoelectrics for power generation devices. As shown in Figure 4(d), for *p*-type $Nd_xYb_yFe_3CoSb_{12}$ MS-SPS samples, we observe a largely enhanced ZT_{ave} than that of SS and TMS-SPS samples, namely, in the temperature range from 300 to 840 K. It is also found that the ZT_{ave} are 0.72, 0.39 and 0.63 for MS-SPS, SS and TMS-SPS samples, respectively. To identify the repeatability of this processing technique, we synthesized another *p*-type skutterudites based on $Nd_xFe_3CoSb_{12}$ compounds with the same preparation route as described in the experimental section for $Nd_xYb_yFe_3CoSb_{12}$ compounds. It turns out to us that the as-prepared bulks possess similar microstructures and their positive impact on electrical transport and phonons transport in $Nd_xFe_3CoSb_{12}$ compounds are also achieved, leading to a maximum *ZT* value up to 0.99 at 770 K for $Nd_{0.9}Fe_3CoSb_{12}$ compound, ~34% enhancement over the SS sample as shown in Figure. S1 of supplementary material. Moreover, for *p*-type $Nd_xFe_3CoSb_{12}$ MS-SPS sample as shown in Figure 4 (d), similarly results show increased ZT_{ave} at temperatures between 300 to 840 K compared to the SS and TMS-SPS samples, i.e., 0.66 *vs.* 0.52 *vs.* 0.63 for MS-SPS, SS and TMS-SPS samples, respectively. As such, we believe that the technique we developed in our study is generally applicable for preparing high performance *p*-type skutterudites compounds.

In summary, *p*-type filled skutterudites $Nd_xYb_yFe_3CoSb_{12}$ (x+y=1.0, x=0.3, 0.4, 0.5, 0.6, 0.7) compounds have been successfully synthesized via a home-made melt spinning system followed by spark plasma sintering within less than 3 h. It is found that an optimized combination of fillers along with the favorable microstructure remarkably decrease the lattice thermal conductivity by introducing different

scattering mechanisms and simultaneously maintain considerable electrical transport properties. These concomitant effects result in an enhanced thermoelectric performance with the dimensionless figure of merit *ZT* value up to 1.02 at 760 K for $Nd_{0.6}Yb_{0.4}Fe_3CoSb_{12}$ MS-SPS sample. Besides, this technique based on the melt-spinning process is believed to be applicable to produce the remaining *p*-type filled skutterudites with high thermoelectric performance. The drastically reduced processing time beyond the enhanced thermoelectric performance will be well suitable for the commercial-scale production for power generation application.

Acknowledgements

The work was financially supported in part by the National Natural Science Foundation of China (Grant no. 11404044, 51472036, 51401202), the Fundamental Research Funds for the Central Universities (CQDXWL-2013-Z010). This work at the Chongqing Institute of Green and Intelligent Technology, Chinese Academy of Sciences is also supported by the 100 Talent Program of the Chinese Academy of Science, Grant No. 2013-46.

[1] C. Uher, ed. T. M. Tritt, Academic Press, San Diego, 69 (2001) 139–253.

[2] T. Caillat, A. Borshchevsky, J. P. Fleurial, J. Appl. Phys. 80 (1996) 4442-4449.

[3] B. X. Chen, J. H. Xu, C. Uher, D. T. Morelli, G. P. Meisner, J. P. Fleurial, T. Caillat, A. Borshchevsky, Phys. Rev. B: Condens. Matter 55 (1997) 1476.

[4] L. D. Chen, T. Kawahara, X. F. Tang, T. Goto, T. Hirai, J. S. Dyck, W. Chen, C. Uher, J. Appl. Phys. 90 (2001) 1864-1868.

[5] H. Li, X. Tang, Q. Zhang, C. Uher, Appl. Phys. Lett. 94 (2009) 102114.

[6] H. Li, X. F. Tang, Q. J. Zhang, C. Uher, Appl. Phys. Lett. 93 (2008) 252109.

[7] D. T. Morelli, G. P. Meisner, J. Appl.Phys.77 (1995) 3777-3781.

[8] X. Zhang, L. D. Zhao, Journal of Materiomics 1 (2015) 92-105.

[9] G. A. Slack,V. G. Tsoukala, J. Appl. Phys. 76 (1994) 1665-1671.

[10] G. A. Slack, CRC Handbook of Thermoelectrics, ed. D. M. Rowe, Boca Raton, FL: CRC, 1995.

[11] B. C. Sales, D. Mandrus, R. K. Williams, Science 272 (1996) 1325-1328.

[12] L. Nodstrom, D. J. Singh, Phys. Rev. B 53 (1996) 1103-1108.

[13] D. T. Moreli, G. P. Meisner, B. X. Chen, S. Q. Hu, C. Uher, Phys. Rev. B 56 (1997) 7376-7383.

[14] B. C. Scaales, D. Mandrus, B. C. Chakoumakos, V. Keppens, J. R. Thomspon, Phys. Rev.B 56 (1997) 15081-15089.

[15] X. Shi, J. Yang, J. R. Salvador, M. F. Chi, J. Y. Cho, H. Wang, S. Q. Bai, J. H. Yang, W. Q. Zhang, L. D. Chen, J. Am. Chem. Soc. 134 (2012) 2842.

[16] L. N. Zhou, P. F. Qiu, C. Uher, X. Shi, D. L.Chen, Intermetallics 32（2013）209-213.

[17] G. J. Tan, S. Y. Wang, X. F. Tang, J. Electron. Mater 43（2014）1712-1717.

[18] R. H. Liu, J. Yang, X. H. Chen, X. Shi, L. D. Chen, C. Uher, Intermetallics 19（2011）1747-1751.

[19] M. G. Kanatzidis, Chem. Mater. 22（2010）648-659.

[20] Q. Jie, J. Zhou, X. Shi, I. K. Dimitrov, Q. Li, arXiv preprint, arXiv:1006（2010）5715.

[21] G. J. Tan, W. Liu, S. Y. Wang, Y. G. Yan, H. Li, X. F. Tang, C. Uher, J. Mater. Chem. A 1（2013）12657-12668.

[22] Y. G. Tang, Sinn-wen. Chen, G. Jeffrey Snyder, Journal of Materiomics 1（2015）75-84.

[23] L. D. Zhao, V. P. Dravid, M. G. Kanatzidis, Energy Environ. Sci. **7**（2014）251.

[24] W. J. Xie, J. A. He, H. J. Kang, X. F. Tang, S. Zhu, M. Laver, S. Y. Wang, J. R. D. Copley, C. M. Brown, Q. J. Zhang, T. M. Tritt, Nano Lett. 10（2010）3283.

[25] X. Y. Zhou, G. Y. Wang, L. Zhang, H. Chi, X. L. Su, J. Sakamoto, C. Uher, J. Mater. Chem. 22（2012）2958-2964.

[26] X. Y. Zhou, G. W. Wang, L. J. Guo, H. Chi, G. Y. Wang, Q. F. Zhang, C. Q. Chen, T.Thompson, Jeff Sakamoto, V. P. Dravid, G. Z. Cao, Ctirad Uher, J. Mater. Chem. A 2（2014）20629-20635.

[27] G. J. Tan, Y. Zheng, X. F. Tang, Appl. Phys. Lett. 103（2013）183904.

[28] T. Dahal, Q. Jie. Y. C. Lan, C. F. Guo, Z. F. Ren, Phys. Chem. Chem. Phys. 16（2014）18170-18175.

[29] J. Zhou, Q. Jie, L. Wu, I. Dmiitrov, Q. Li, X. Shi, J. Mater. Res. 26（2011）184-1847.

Captions for Figures

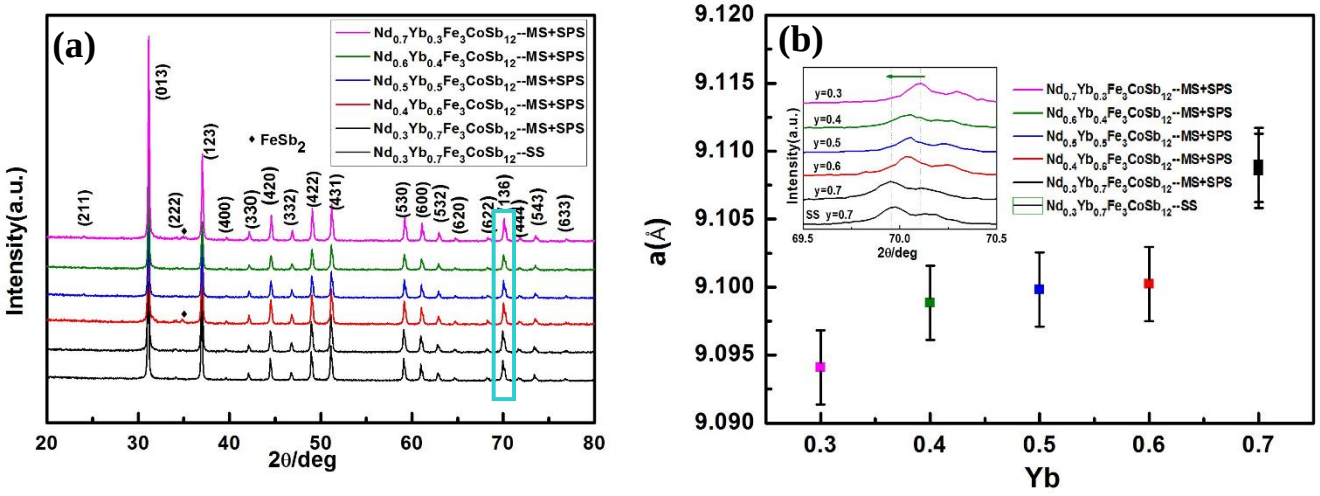

Figure 1. (a) XRD patterns of $Nd_xYb_yFe_3CoSb_{12}$ bulk samples prepared by MS-SPS and SS, respectively; (b)The lattice parameter of $Nd_xYb_yFe_3CoSb_{12}$ compounds prepared by MS-SPS and SS.

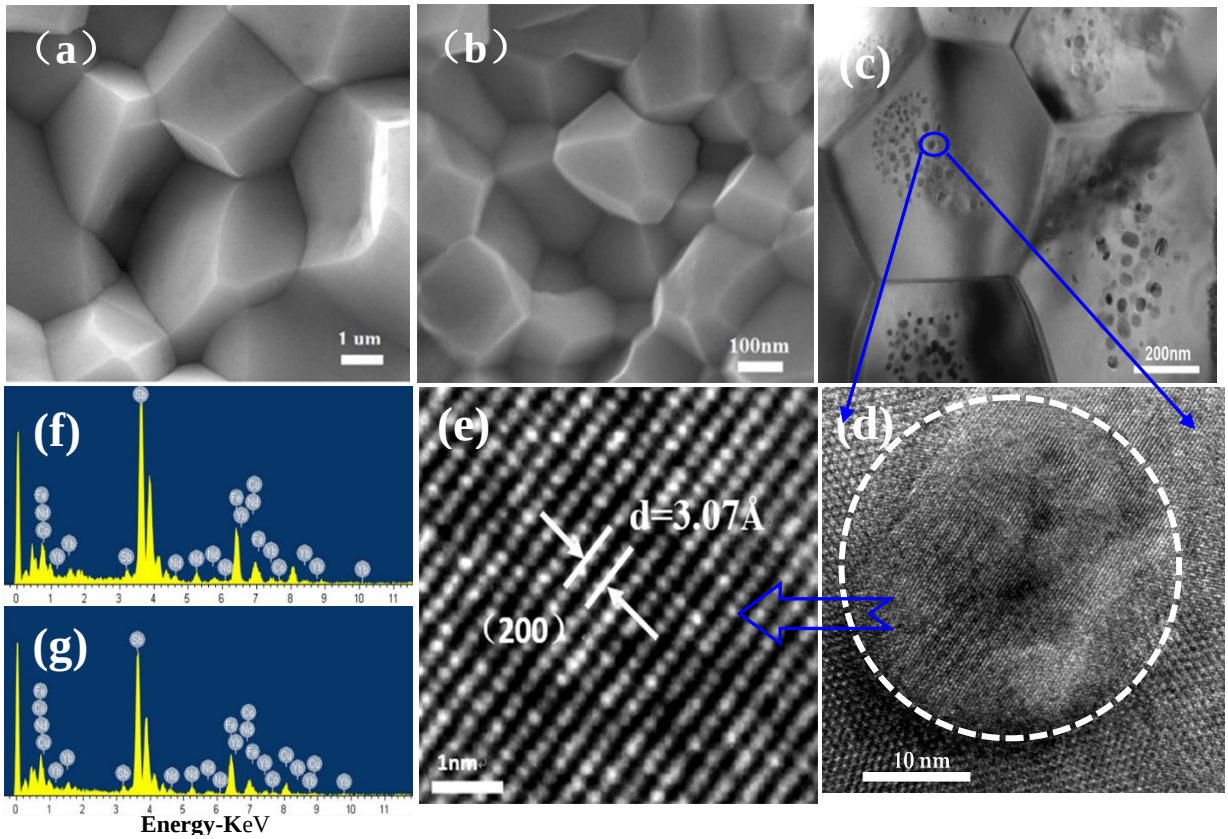
（a）
1 um
（b）
100nm
(c)
200nm
(f)
(g)
(e)
d=3.07Å
（200）
1nm
(d)
10 nm
Energy-KeV

Figure 2. (a) and (b) show the typical SEM images of $Nd_{0.3}Yb_{0.7}Fe_3CoSb_{12}$ compounds prepared by SS and MS-SPS, respectively; (c) displays the low-magnification transmission electron microscopy (HRTEM) of the MS-SPS sample $Yb_{0.3}Nd_{0.7}Fe_3CoSb_{12}$, (d) a representative HRTEM image of one spherical/ellipsoidal precipitate, (e) enlarged HRTEM showing the precipitate phase of the MS-SPS sample $Yb_{0.3}Nd_{0.7}Fe_3CoSb_{12}$, (f) and (g) are the EDS results from matrix and nanoscaled precipitate, respectively.

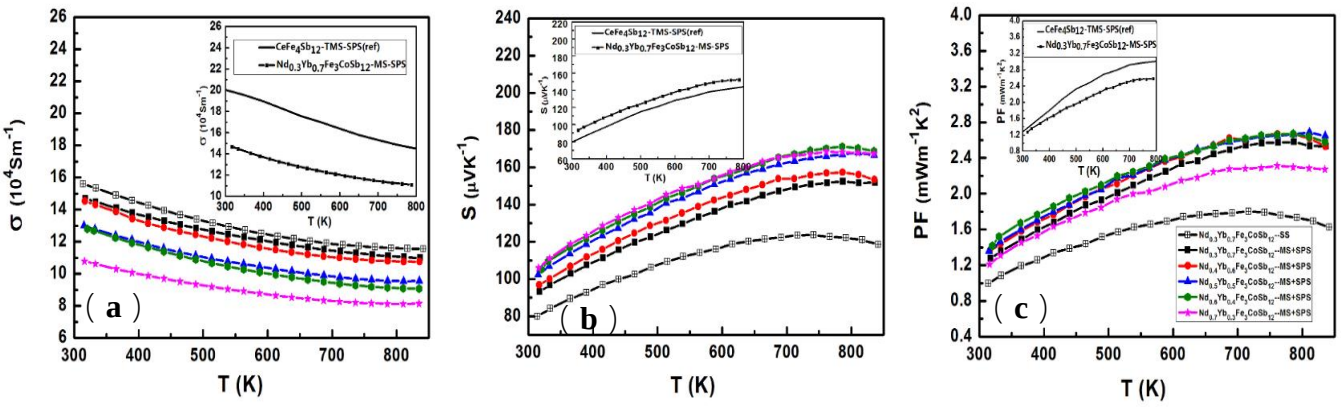

Figure 3. Temperature dependence of (a) electrical conductivity, (b) Seebeck coefficient, (c) power factor of $Nd_xYb_yFe_3CoSb_{12}$ compounds (x+y=1.0, x=0.3, 0.4, 0.5, 0.6, 0.7) prepared by SS and MS-SPS, respectively. The above insets are the comparison of the electrical transport performance for $CeFe_4Sb_{12}$ and $Nd_{0.3}Yb_{0.7}Fe_3CoSb_{12}$ compounds prepared by TMS-SPS and MS-SPS.

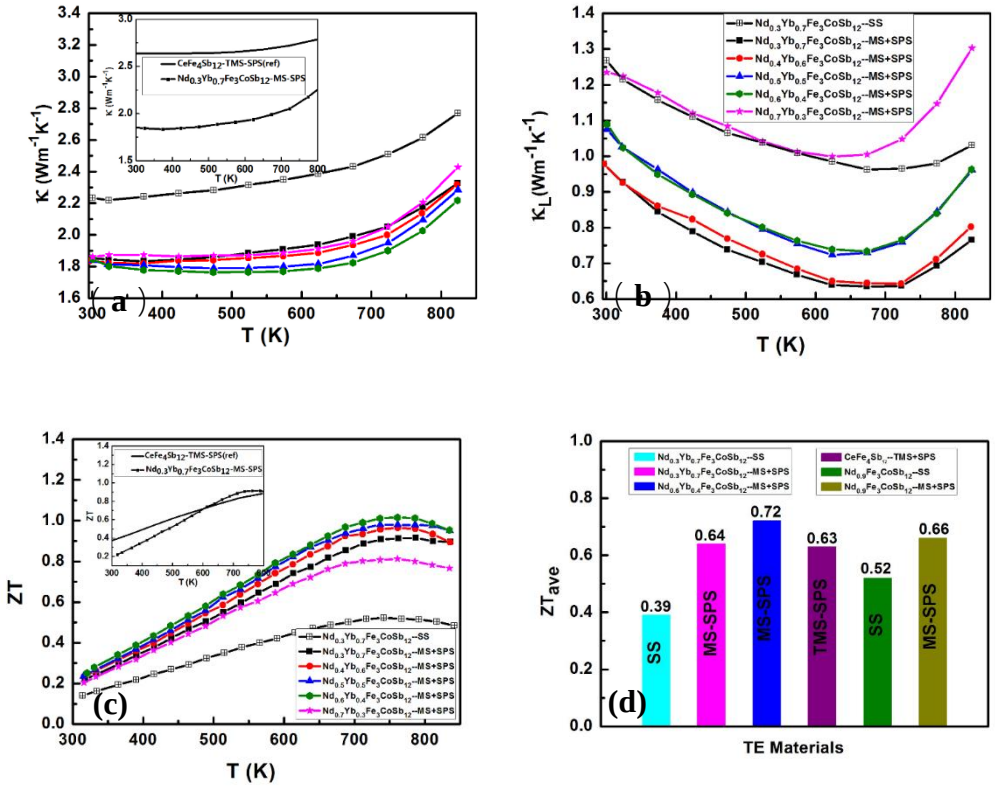

Figure 4. Temperature dependence of (a) thermal conductivity (κ), (b) lattice thermal conductivity(κ_l),

(c) *ZT* of $Nd_xYb_yFe_3CoSb_{12}$ compounds (x+y=1.0, x=0.3, 0.4, 0.5, 0.6, 0.7) prepared by SS and MS-SPS, respectively. Temperature dependence of (d) ZT_{ave} for $Nd_xYb_yFe_3CoSb_{12}$ / $Nd_xFe_3CoSb_{12}$ / $CeFe_4Sb_{12}$ compounds between 300 K to 840 K prepared by MS-SPS , SS and TMS-SPS, respectively.

Table caption

Table I. Room temperature thermoelectric properties of $Nd_xYb_yFe_3CoSb_{12}$ compounds prepared by SS and MS-SPS.

Nominal composition	σ (10^5S m^{-1})	n (10^{21}cm^{-3})	μ (cm^{2}V^{-1}s^{-1})	*S* (μV K^{-1})	k (Wm^{-1} K^{-1})	k_L (Wm^{-1} K^{-1})
$Nd_{0.3}Yb_{0.7}Fe_3CoSb_{12}$	1.47	4.26	2.16	93.23	1.85	0.97
$Nd_{0.4}Yb_{0.6}Fe_3CoSb_{12}$	1.45	3.85	2.35	96.87	1.84	0.98
$Nd_{0.5}Yb_{0.5}Fe_3CoSb_{12}$	1.30	3.23	2.52	102.27	1.83	1.08
$Nd_{0.6}Yb_{0.4}Fe_3CoSb_{12}$	1.28	3.13	2.56	105.18	1.85	1.09
$Nd_{0.7}Yb_{0.3}Fe_3CoSb_{12}$	1.08	3.40	1.99	105.98	1.86	1.24
SS-$Nd_{0.3}Yb_{0.7}Fe_3CoSb_{12}$	1.56	4.20	2.32	79.92	2.23	1.27

Supplementary Information

Melt Spinning Synthesis of *p*-type Skutterudites: Drastically Speed Up the Process of High Performance Thermoelectrics

Lijie Guo[a], Guiwen Wang[a], Kunling Peng[a,b], Yanci Yan[a], Xiaodan Tang[a], Min Zeng[c,d], Jiyan Dai[c], Guoyu Wang[b], Xiaoyuan Zhou*[a]*

[a]College of Physics, Chongqing University, Chongqing 401331, People's Republic of China.

[b]Chongqing Institute of Green and Intelligent Technology, Chinese Academy of Sciences, Chongqing 400714, People's Republic of China.

[c]Department of Applied Physics, The Hong Kong Polytechnic University Kowloon, Hong Kong.

[d]Institute for Advanced Materials and Guangdong Provincial Key Laboratory of Quantum Engineering and Quantum Materials，South China Normal University, Guangzhou 510006, China.

*To whom correspondence should be addressed:
Author Email: xiaoyuan2013@cqu.edu.cn; guoyuw@cigit.ac.cn

1. Temperature dependence of electronic thermal conductivity (κe) of NdxYbyFe3CoSb12 compounds (x+y=1.0, x=0.3, 0.4, 0.5, 0.6, 0.7) prepared by MS-SPS and SS, respectively.

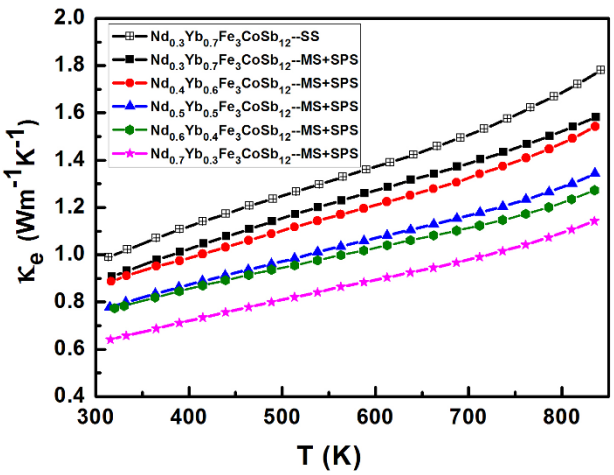

Figure. S1. Temperature dependence of electronic thermal conductivity (κe) of $Nd_xYby Fe_3CoSb_{12}$ compounds (x+y=1.0, x=0.3, 0.4, 0.5, 0.6, 0.7) prepared by MS-SPS and SS, respectively.

2. Temperature dependence of *ZT* for $Nd_xFe_3CoSb_{12}$ compounds (x=0.8, 0.85, 0.9, 0.95, 1.0) prepared by MS-SPS and SS, respectively.

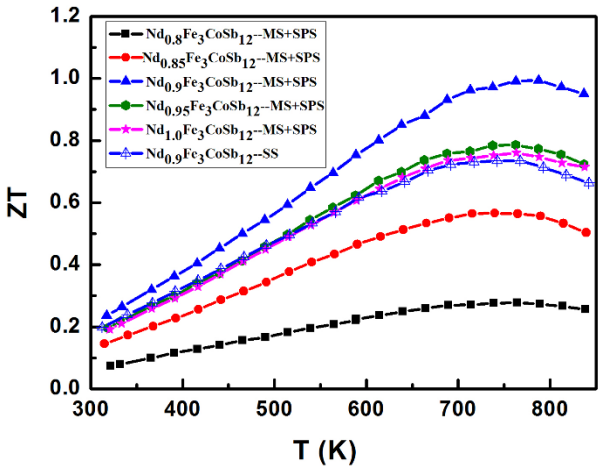

Figure. S2. Temperature dependence of *ZT* for $Nd_xFe_3CoSb_{12}$ compounds (x=0.8, 0.85, 0.9, 0.95, 1.0) prepared by MS-SPS and SS, respectively.